

# ESTIMATING IMPERVIOUS SURFACE FOR THE URBAN AREA EXPANSION: EXAMPLES FROM CHANGCHUN, NORTHEAST CHINA

Dongmei Lu<sup>1,2</sup>, Kaishan Song<sup>3,2\*</sup>, Lihong Zeng<sup>3</sup>, Dianwei Liu<sup>3</sup>, Shahbaz Khan<sup>2</sup>, Bai Zhang<sup>3</sup>, Zongming Wang<sup>3</sup>, Cui Jin<sup>3</sup>

<sup>1</sup> Computer Science and Engineering College, Jilin Architectural and Civil Engineering Institute, Hongqi Street 1129, Changchun 130021, Jilin Province, PR China.

<sup>2</sup> Land and Water, CSIRO, Charles Sturt University, Building 24, Locked bag 558, Wagga Wagga, NSW Australia

<sup>3</sup> Northeast Institute of Geography and Agricultural Ecology, Chinese Academy of Sciences, No.3195, Weishan Road, Changchun 130012, Jilin Province, PR China.

Corresponding author: songks@neigae.ac.cn; Tel: +86-431-85542364

**KEY WORDS:** Changchun, remote sensing, estimation, impervious, land-use, classification.

## ABSTRACT:

As a developing country, China is now undergoing a quick process of urbanization. Therefore, understanding and managing the urban environment is a prerequisite for addressing sustainability, which is an increasingly important issue need a range of discipline to cope with. This paper explored extraction of impervious surface information from Landsat ETM+ data with the integration of fraction images from linear spectral mixture analysis based upon Ridd's vegetation-impervious surface-soil (V-I-S) model. A new approach for urban land-use classification, based on the combined use of impervious surface and spectral mixture analysis (SMA) were applied in this paper. The minimum noise fraction transform (MNF) procedure was applied to transform the six reflective bands into a new coordinate set to select the four endmembers, e.g. high-albedo surface, low-albedo surface, soil and vegetation.. Results showed that the integration of fraction images improved urban impervious surface estimation. The impervious surface in the urban area were derived from high-albedo surface and low-albedo surface. Accuracy assessment indicated that the root-mean-square error is less than 10.2% for the impervious surface image. The main factors that affect the accuracy are the reflectance variation caused by atmospheric factors, sun-sensor-target geometry. How to deal with these factors to minimize reflectance variation will be the future study topics. Also water body and shade were not addressed in this paper, which also need to be considered in the future study.

## 1. INTRODUCTION

Urbanization is perhaps one the most important human activities, creating enormous impacts on the environment at the local, regional and global scales (Turner et al., 1990). Although urbanization, the form of land cover (built-up or impervious surface) occupies less than 2% of the global land surface, many evidence show that human disturbance due to urbanization has significantly altered the natural landscape (Grubler, 1994). Therefore, understanding and managing the urban environment is a prerequisite for addressing sustainability, an increasingly important issue across a range of disciplines (Newman & Kenworthy, 1999). Improving urban land-use/cover classification accuracy has been an important issue in remote sensing literature (Liu and Wen, 2004). Different approaches have been applied, which include incorporation of geographic data, census data, texture feature and structure or contextual information into remote sensing spectral data. Furthermore, expert systems, fuzzy classification, and merged multi-sensor data for improving spatial resolution have been applied. However, urban land-use/cover classification is still a challenge with medium or coarse spatial resolution remotely sensed data due to the large number of mixed pixels and the spectral confusions among different land-use/cover types.

Recent institutional changes, marketization and globalization combined together have brought about new processes of rural-urban interaction, giving rise to new forms of human settlements in china, especially after Chinese reform and open policies were carried out since 1978. The latest national population census conducted in 2000, revealed an accelerated rate of urbanization, characterized both by its scale and change

speed that have no parallel elsewhere in the world (Tian et al., 2005). China owns the largest population (1.265 billion) in the world, of which 456 million (36%) live in cities and towns (State Council of China Office of Population Census 2001). Urbanization in China has speeded up, urban population only comprise 20% of the whole country population in 1982, while it has reached 36% in year 2000. A net gain of 16% took place in less than 20 years, which cause a sharp contrast o the pre-reform era, when the urban population only increased 7.1% over 30 year period (Zhang and Zhao, 1998; Tian et al., 2005). Rapid urban growth was mainly attributed to migration form the countryside to cities and town, the conversion from rural administrative units to city units, and the natural urban population increase, and all the driving force can be traced from economic development.

The focus of this study is to examine urban LULC patterns by SMA method based upon V-I-S model. Changchun (Jilin provincial Capital city), the third largest city in northeast China, has been chosen as the area of study. With over 3.58 million populations live in the urban area, the city is the nation's automobile capital of the nation. 3 scenes Landsat TM and ETM+ image since 1993 that covers the City were used in conjunction with other types of spatial data for the analysis city LULC for city expansion study. Specific objectives of this research are: (1) employing V-I-S model to derive landscape fractional components, and to apply them to characterize the urban expansion; (2) exploring the urban area expansion process from 1993 to 2004 based upon V-I-S model and analyzed the possible driving forces.

## 2. STUDY AREA

Changchun is the capital and largest city of Jilin province, located in the northeast of China. It is the largest centre for China's automotive industry. As of 2007, Changchun has a population of 7.45 million, including counties and county-level cities. The urban districts have a total population of 3.58 million. Changchun has incredibly cold, long winters with the temperature dropping as low as -30°C; and the temperature sometimes goes up 35 °C in late July in summer. Changchun in its present form is a new city with only about 200 years of history. Figure.1 showed the urban expansion from 1905 to 1993. It expanded rapidly as the junction between the Japanese-owned South Manchurian Railway and the Russian-owned Chinese Eastern Railway from 1905-1935. In 1932, Changchun became the capital of Manchukuo, which existed from 1931 to 1945. The city underwent rapid expansion in both its economy and infrastructure. Changchun became the capital of Jilin Province, P.R China in 1954. As Changchun's main industry, the manufacturing of transportation facilities and machinery such as those of automobile, passenger train, and tractor has developed very well. Industries such as machinery, electronics, optics, chemistry, medicine, textile, metallurgy, building materials and foodstuffs all assume their own features and advantages.

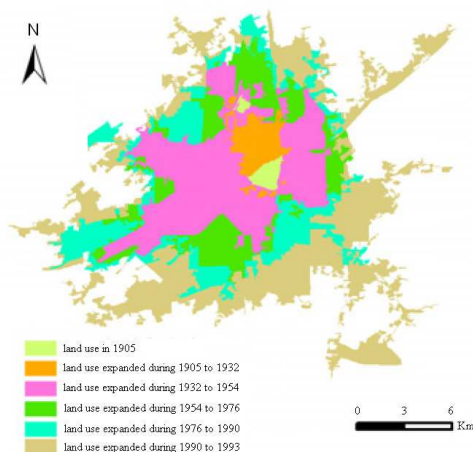


Figure.1 The expansion of Changchun urban area from 1905 to 1993

## 3. MATERIAL AND METHODOLOGIES

### 3.1 Landsat image processing

3 sub-scenes of Landsat 5 TM and Landsat 7 ETM+ image (path 118/row 28, 29) of Changchun, China, which acquired on the 23 August 1993, the 18 September 2000 and 23 August 2003, were used in this research. Images were processed by Remote Sensing Ground Station, Chinese Academy of Sciences (RSGS). Possible geo-position errors due to terrain effects were corrected using the ortho-correction method based on DEM, which derived from digitized topographic map with 1:5,000 scales. All images were rectified to a common Universal Transverse Mercator coordinate system. Bands 1 through 5 and band 7 were utilized at a spatial resolution of 30 m.

### 3.2 Determination of reflectance from TM and ETM+

The digital numbers (DN) of the TM image were converted to normalized exo-atmospheric reflectance measures following the methods proposed by Markham and Barker (1987). The calibration parameters for Landsat-7 ETM+ were obtained from the ETM+ data header (Irish, 1998). We assumed homogeneous atmospheric conditions within the image, so no atmospheric corrections were performed.

### 3.3 Spectral mixture analysis

Spectral mixture analysis (SMA) was utilized for calculating land cover fractions within a pixel and involves modeling a mixed spectrum as a combination of spectra for pure land cover types, called endmembers (Roberts et al., 1998). The linear spectral mixture model describes the surface composition in each pixel of an image using two to six endmembers (for an ETM+ image). Each endmember represents a pure land cover type. The linear mixture model is:

$$R_j = \sum_{i=1}^N f_i R_{ij} + e_j \quad (1)$$

Where

$$\sum_{i=1}^N f_i = 1 \text{ and } f_i \geq 0 \quad (2)$$

where  $R_j$  is the reflectance for each band  $j$  in the ETM+ image,  $N$  is the number of endmembers,  $f_i$  is the fraction of endmember  $i$ ,  $R_{ij}$  is the reflectance of endmember  $i$  in band  $j$ , and  $e_j$  is the unmodeled residual. Model fitness is normally assessed by the residual term  $e_j$  or the RMS over all image bands ( $M$ ):

$$RMS = \left( \sum_{j=1}^M e_j / M \right)^{1/2} \quad (3)$$

The fraction of each endmember can be obtained by applying a least squares technique in order to minimize the unmodeled residual error  $e_j$ , given the constraints on  $f_i$ . As stated by Small (2001), the linear mixture model may not be appropriate for applications in which only subtle spectral differences exist in all sampled bands. In many applications, about three to four endmembers are chosen for simple linear mixture models (Roberts et al., 1993; Small, 2001).

### 3.4 Endmember selection methods

One approach for choosing image endmembers is selecting representative homogeneous pixels from satellite images through visualizing spectral scatter plots of image band combinations (Rashed et al., 2001). In this study, the maximum noise fraction (MNF) transformation was applied to trace the endmember (Wu & Murray, 2003). The first three components were shown in Fig.2. Previous research has shown that use of MNF transform can improve the quality of fraction images (Wu & Murray, 2003). The first four components were retained for use in the LSMA models, while the last two components discarded due to the high proportion of noise content. Four endmembers were selected in this study; they are bright albedo surface, dark albedo surface, soil and vegetation (Fig.3). These endmembers were initially identified from the images based on ground truth and high-resolution aerial photographs, and then the reflectances of these initial endmembers were compared with the endmembers selected from the scatterplot of combination MNF1-3. The endmembers with similar MNF

spectra at the extreme vertices of the scatterplots were selected (see figure.3a-c).

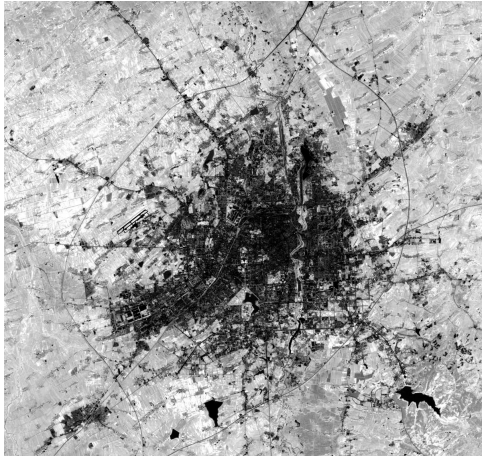


Figure.2a MNF component1

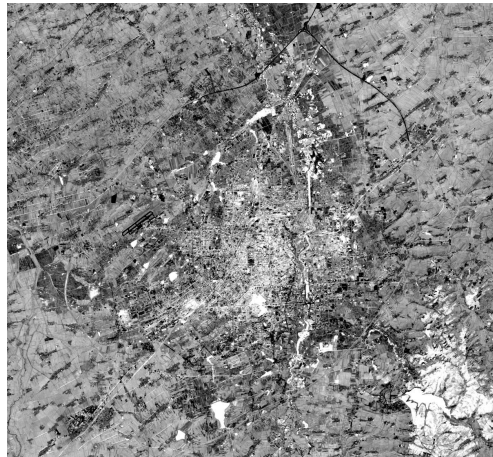


Figure.2b MNF component2



Figure.2c MNF component3

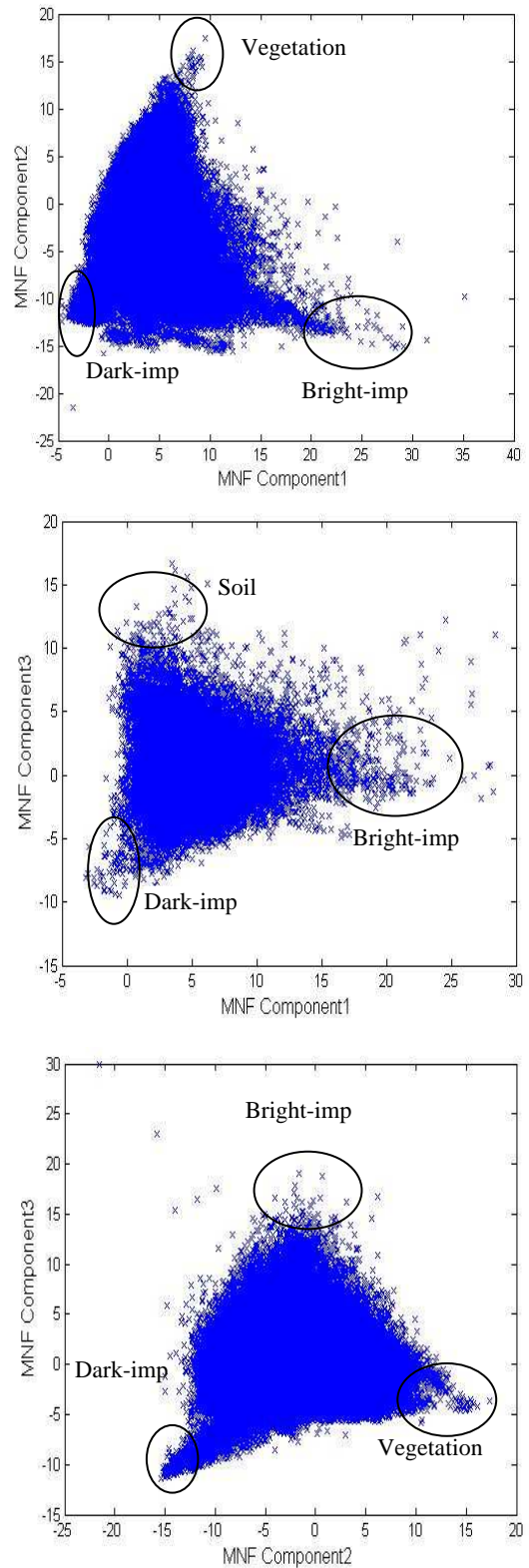


Figure.3 Feature space represents the first three MNF components. The extreme pixel clusters which bound almost all other pixels in these three feature spaces were delineated as endmembers. High albedo (e.g. concrete, clouds, and sand), low albedo (e.g. water, shade and asphalt), vegetation (e.g. crop, grass and trees), and soil (e.g. bare soil and quarry), were identified according to these feature spaces and their corresponding features obtained from original reflectance data.

#### 4. RESULTS AND DISCUSSION

##### 4.1 Urban fraction mapping

The endmember fractions were calculated by solving a fully constrained four-endmember linear mixing model using the Landsat TM or ETM+ reflectance data, and the final result were shown in Fig.4~6 for 1993, 2000 and 2003, respectively. The vegetation fraction image correlates with known vegetated areas within the original TM or ETM+ image. From Fig.4a it can be seen that bright albedo surface mainly distributed in urban region, especially in the CBD region, and for there was some haze over the urban region in 1993, which also reflected in the un-mixing result of impervious surface. The low albedo surface also mainly distributed in urban area (Fig. 4b), it included water bodies in this study. But it is more reasonable to mask out water bodies in the future study. The vegetation fraction is near zero in the urban region, while increasing to 10–20% in high-density residential areas, and 20–30% in low-density residential areas, and it is about 70-90% in vegetated areas, nearly 100% only in a small part of crop area (Fig. 4c). Moreover, the soil fraction image is also consistent with the soil distribution in the study area because the soil fraction in the CBD and residential areas is 10–20% but higher than 60% in some parts of the urban fringe (Fig. 4d), where new constructions sites located. Fraction images of dark albedo and high albedo cannot be directly interpreted from the image.

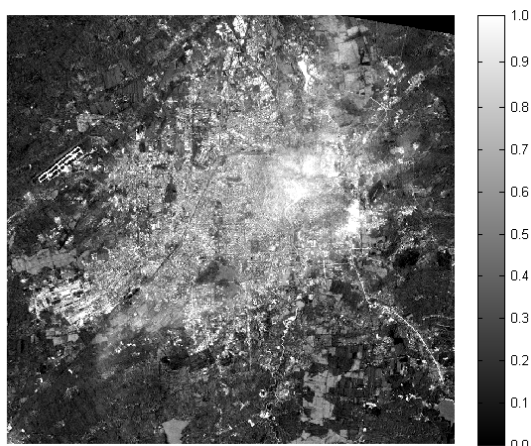


Figure.4a Fraction image of high albedo in 1993

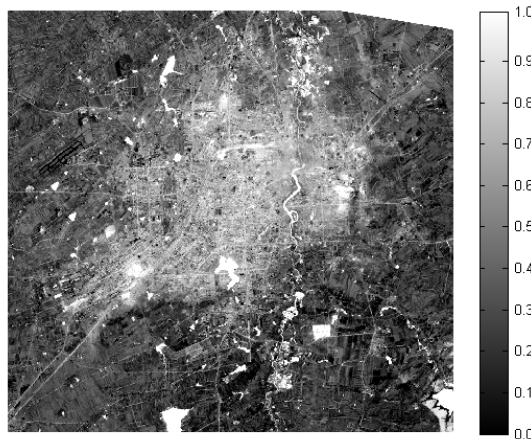


Figure.4b Fraction image of low albedo in 1993

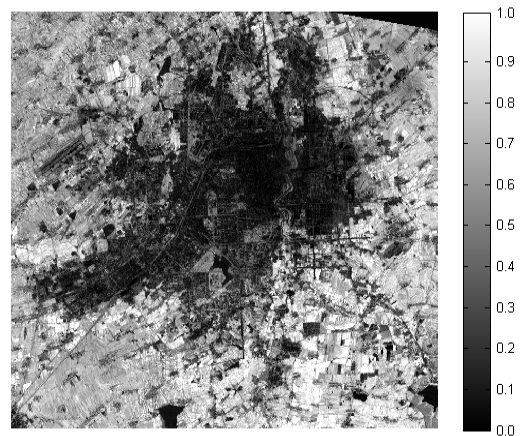


Figure.4c Fraction image of vegetation in 1993

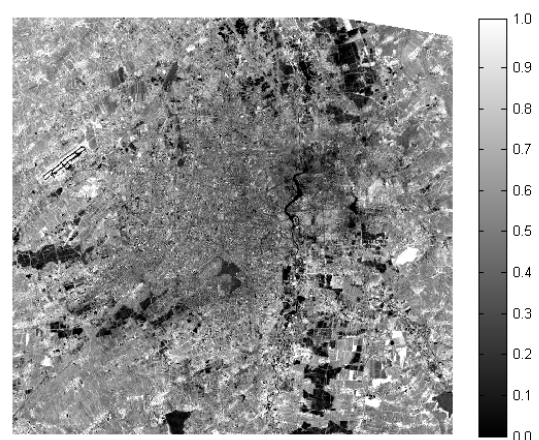


Figure.4d Fraction image of soil in 1993

However, their relationship with impervious surfaces will be built using a two-endmember linear mixture model in this study. Fig. 4 also shows that this model performance is not as good for modeling some high albedo materials, such as high reflectance roofs, clouds, and sand

From Fig.5, it can be seen that the four endmember fractions show the similar trend as that from 1993. It can be easily noticed that high albedo fraction is more evenly distributed in the urban area as no haze disturbance in the original image. While the low albedo surface fraction distributed in most parts of the city, especially in CBD and residential area, also included some water bodies. Most part of urban area is higher than 60%, some area even higher than 80%. This indicates that the building roof or road materials are dark color in Changchun. From Fig.5c, it can be seen that only some parks and area along Yitong River have high values, but in most of the urban area, it is only about 10%, but in the suburban area, especially in the cropping area and forest area, the vegetation fraction is about 70%, only a small vegetable field has high value. This is because the image acquired in late September, so most of the crop is nearly ready for harvest, only irrigated vegetable at their highest cover with sufficient water supply and no sign of chlorophyll lack. Soil fraction has high values in some region, including construction sites, quarries and bare soil regions. But in most of the region, it has a value about 30%, one reason is that Changchun locates in black soil region, the soil spectral reflectance is low compared with most of the other soils, so its reflectance signature is quite close to some of the low albedo surface, also most of the crop in their senescence

stage, also show dark color, that may explain why soil fraction have no obvious distinctive pattern.

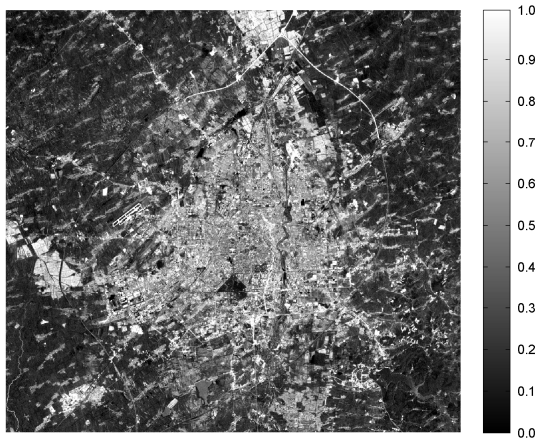


Figure.5a Fraction image of high albedo in 2000

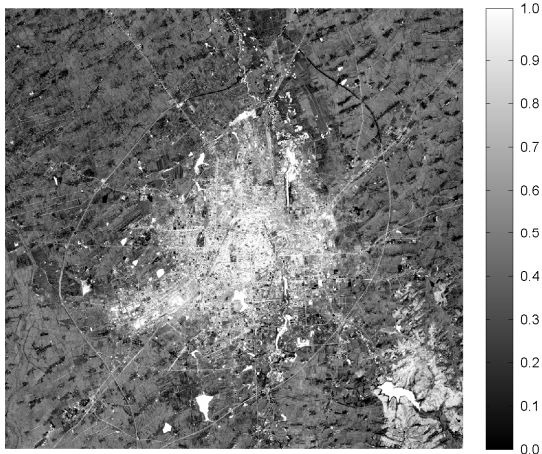


Figure.5b Fraction image of low albedo in 2000

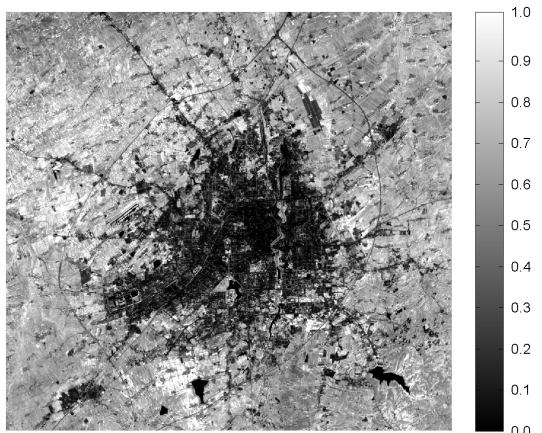


Figure.5c Fraction image of vegetation in 2000

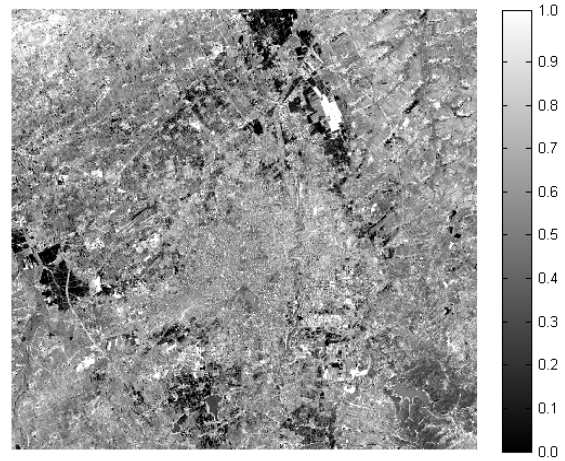


Figure.5d Fraction image of soil in 2000

From Fig.6a-b, it can be seen that high albedo and low albedo fraction have the similar distribution pattern in most parts of the city, especially in CBD and residential area as that from previous years. From Fig.5c, it can be seen that vegetation fraction value is about 80% in most of the cropping area and forest area because this image acquired in late August 2003 when vegetation is just begin to senesce. Soil fraction has also have similar trend, but with low value in the croppin area and forest.

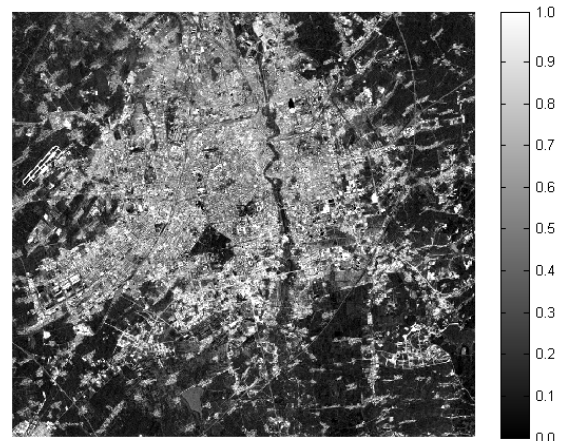


Figure.6a Fraction image of high albedo in 2003

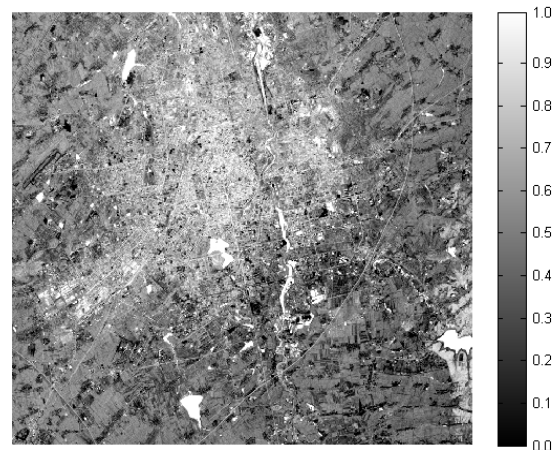


Figure.6b Fraction image of low albedo in 2003

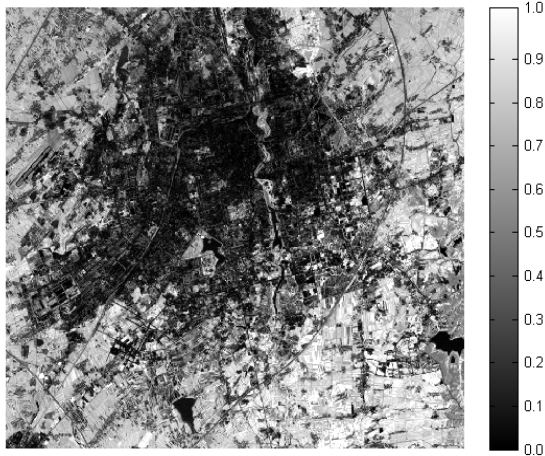


Figure.6c Fraction image of vegetation in 2003

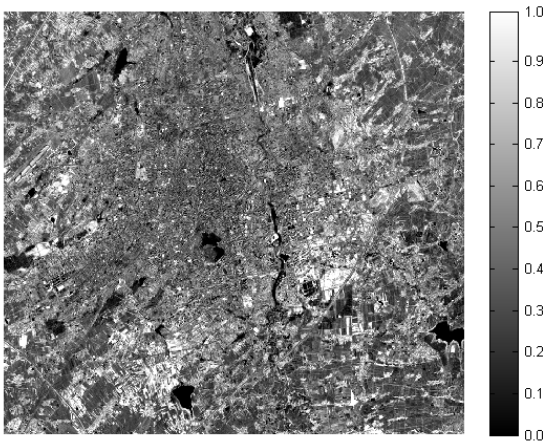


Figure.6d Fraction image of soil in 2003

#### 4.2 Assessment of unmixing model based up V-I-S

The RMS for every image pixel was calculated in order to assess the performance of LSMA model (Table.1 and Figure.7). The mean RMS over the image is 0.0042, 0.0028 and 0.0034, respectively, which suggests a generally good fit (less than 0.015). The RMS images show that this model represents residential, vegetation, soil, and water cover types very well. However, performance is not as good for modeling some high albedo materials, such as high reflectance roofs, clouds, and sand. Also some dark pine forest can not modeled well for their spectral variation from that of deciduous tree (not demonstrated in this paper). Figure.7 only the distribution characteristics of RMS in 2003, it can be seen that RMS value is generally less than 0.015.

Table.1 Unmixing modled RMSE values

| year | Min    | Max    | Mean   | Stdev  |
|------|--------|--------|--------|--------|
| 1993 | 0.0000 | 0.1100 | 0.0042 | 0.0022 |
| 2000 | 0.0000 | 0.0943 | 0.0028 | 0.0018 |
| 2003 | 0.0000 | 0.1238 | 0.0034 | 0.0025 |

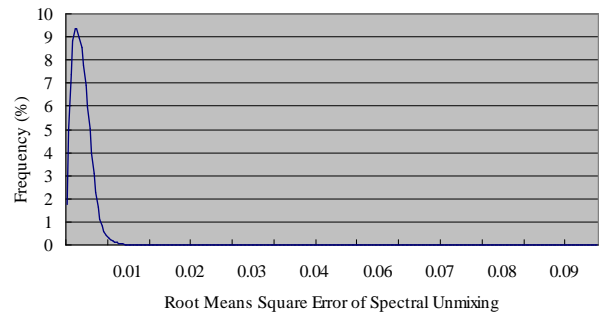


Figure.7 Distribution of Unmixing RMSE

#### 4.3 Impervious surface mapping

According to Wu and Murray's study (2003), impervious surface is likely on or near the line connecting the low albedo and high albedo endmembers in the feature spaces. In other words, most impervious surfaces might be represented by low and high albedo endmembers as follows.

$$R_{imp} = f_{low} \times R_{low} + f_{high} \times R_{high} + e_b \quad (4)$$

$R_{imp,b}$  is the reflectance spectra of impervious surfaces for band  $b$ , and  $f_{low}$  and  $f_{high}$  are the fractions of low albedo and high albedo, respectively.  $R_{low,b}$  and  $R_{high,b}$  are the reflectance spectra of low albedo and high albedo for band  $b$ , and  $e_b$  is the unmodeled residual. Associated with determining  $R_{imp,b}$  is the requirement  $f_{low} + f_{high} = 1$  and  $f_{low}, f_{high}$  great or equal to 0.

In this study, we also applied this methodology proposed by Wu and Murray (2003) to map the impervious surface. We applied this model to build a relationship between impervious surfaces and high and low albedo materials with formula (4) to derive the impervious surface in the urban area of Changchun. Also water bodies were masked out in the final result. The final impervious surface in 2000 and 2003 were shown in figure.8. It can be seen that in the urban area, the impervious surface is quite consistent, the fraction value is about 0.7 in most of the urban area, while in the CBD area it can reach 0.9. This indicates that V-I-S model with LSMA is suitable for urban impervious surface study. As there was some haze in the original image in 1993 that affected the modeling result, impervious surface area was not shown in the final result.

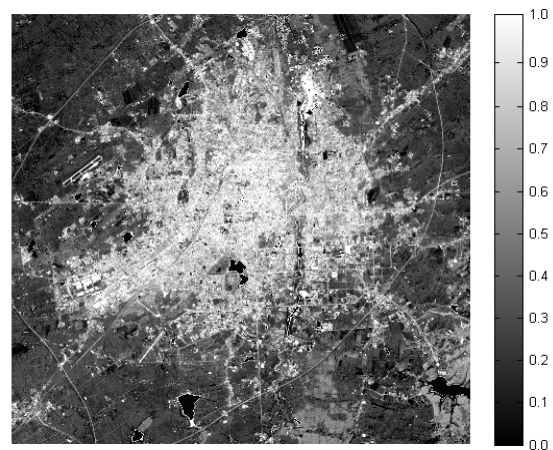


Figure.8a Impervious surface in 2000

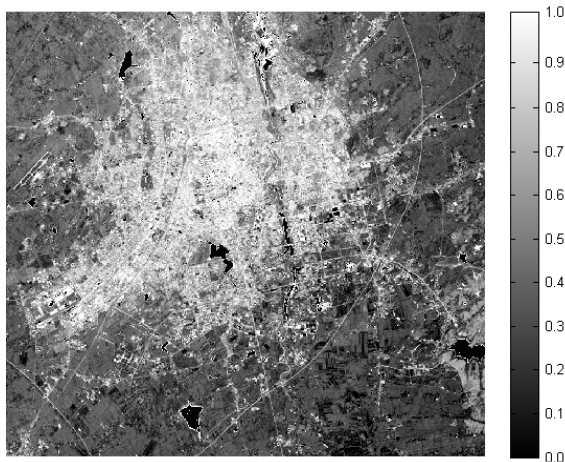


Figure.8b Impervious surface in 2003

## 5. CONCLUSION AND FUTURE RESEARCH

In this paper, a LSMA method was applied to quantify urban composition under the framework of V-I-S model. MNF method was applied for the acquired image to select the endmembers, and a linear spectral mixture analysis method was developed to derive the fractions of green vegetation, high albedo and low albedo, and soil. The impervious surface was derived from high albedo and low albedo surface. It can be concluded that the LSMA model is reasonable to retrieve urban impervious surface in our study case; V-I-S model can be used to monitoring urban expansion, especially for city impervious area estimation. One future research direction could be the accuracy assessment of the vegetation and soil fraction. Contemporaneous high-resolution images, such as Quickbird or IKONOS imagery, should be helpful to obtain ground truthing information of vegetation and soil. Also, how to deal with spectral variation caused by sun-object-sensor geometry is not delivered in this paper, which needs to be coped with in future study, especially with consideration of urban dynamics study.

### Acknowledgements

We would like to thank Dr. Yuanzhi Zhang from the Chinese University of Hongkong and Dr. Mohsin Hafeez from Charles Sturt University, Australia for their help and valuable comments on this work. Financial Support from NEIGAE frontier research project (k08y44) is also acknowledged.

### References

Grubler, A., 1994. Technology. In changes in land use and land cover: *A global perspective*. pp. 287-328. Cambridge University Press, Cambridge.

Guangjin, Tian., Jiyuan, Liu., Yichun, Xie., Zhifeng, Yang., Dafang, Zhuang., Zheng, Niu., 2005. Analysis of spatio-temporal dynamic pattern and driving factors of urban land in China in 1990s using TM images and GIS. *Cities*, 22(6), pp. 400-410.

Irish, R., 1998. Chapter 11: Data product. Landsat 7 science data users handbook.

Lu, D., & Weng, Q., 2004. Spectral mixture analysis of the urban landscape in Indianapolis city with Landsat ETM+ imagery. *Photogrammetric Engineering & Remote Sensing*, 70(9), pp. 1053–1062.

Markham, B. L., Barker, J. L., 1987. Thematic Mapper bandpass solar exoatmospheric irradiances. *International Journal of Remote Sensing*, 8, pp. 517–523.

Newman, P., Kenworthy, J., 1999. *Sustainability and cities: overcoming automobile dependence*. Washington, DC: Island Press.

Rashed, T., Weeks, J. R., & Gadalla, M. S., 2001. Revealing the anatomy of cities through spectral mixture analysis of multispectral satellite imagery: a case study of the greater Cairo region, Egypt. *Geocarto International*, 16(4), pp. 5 – 15.

Ridd, M. K., 1995. Exploring a V-I-S (vegetation-impervious surface-soil) model for urban ecosystem analysis through remote sensing: comparative anatomy for cities. *International Journal of Remote Sensing*, 16, pp. 2165–2185.

Roberts, D. A., Gardner, M., Church, R., Ustin, S., Scheer, G., Green, R. O., 1998. Mapping chaparral in the Santa Monica Mountains using multiple endmember spectral mixture models. *Remote Sensing of Environment*, 65, pp. 267–279.

Small, C., 2002. Multitemporal analysis of urban reflectance. *Remote Sensing of Environment*, 81, pp. 427–442.

State Council of China Office of Population Census., 2001. *China Population Census*. Beijing: Statistical Press of China.

Stefanov, W. L., Ramsey, M. S., Christensen, P. R., 2001. Monitoring urban land cover change: an expert system approach to land cover classification of semiarid to arid urban centers. *Remote Sensing of Environment*, 77, pp. 173–185.

Stuckens, J., Coppin, P. R., Bauer, M. E., 2000. Integrating contextual information with per-pixel classification for improved land cover classification. *Remote Sensing of Environment*, 71, pp. 282–296.

Thomas, N., Hendrix, C., Congalton, R. G., 2003. A comparison of urban mapping methods using high-resolution digital imagery. *Photogrammetric Engineering and Remote Sensing*, 69, pp. 963–972.

Turner, B L II, Clark, W C and Kates, R W, et al., 1990. *The earth as transformed by human action: global and regional change in the biosphere over the past 300 years*. Cambridge University Press, Cambridge.

Wu, C., & Murray, A. T., 2003. Estimating impervious surface distribution by spectral mixture analysis. *Remote Sensing of Environment*, 84, pp. 493–505.

Zhang, L and Zhao, S., 1998. Re-examining China's 'Urban' concept and the level of urbanization. *The China Quarterly*, 154, pp. 330-381.

